Sensors and Materials, Vol. 29, No. 4 (2017) 405–410
MYU Tokyo

S & M 1333

Simulation of Solidly Mounted Resonator Using Mason Model and Its Implementation

Wei-Che Shih, Ying-Chung Chen, Chien-Chuan Cheng,[1] Kuo-Sheng Kao,[2*]
Da-Long Cheng,[2] Po-Wei Ting, and Huan-Hsien Yeh[2]

Department of Electrical Engineering, National Sun Yat-Sen University,
70 Lienhai Rd., Kaohsiung 80424, Taiwan R.O.C.
[1]Department of Electronic Engineering, De Lin Institute of Technology,
No. 1, Ln. 380, Qingyun Rd., Tucheng Dist., New Taipei City 236, Taiwan R.O.C.
[2]Department of Computer and Communication, Shu-Te University,
No. 59, Hengshan Rd., Yanchao, Kaohsiung County 82445, Taiwan R.O.C.

(Received August 30, 2016; accepted December 22, 2016)

Keywords: frequency tuning, acoustic wave device, simulation, Mason model

Acoustic wave devices are divided into two categories: surface acoustic wave (SAW) and bulk acoustic wave (BAW) devices. To provide modification parameters during manufacturing, advanced modeling, simulation, and other computational methods is crucial for maintaining a competitive edge through efficient product design. In this study, an equivalent circuit modification based on the Mason model is used for obtaining the actual device measurements. The effects of various film conditions, material properties, and geometrical variations on resonator performance are investigated. Furthermore, the performance of a filter comprising various stages of series and parallel resonators is examined.

1. Introduction

Bulk acoustic wave (BAW) devices have been widely used in wireless communication applications such as Bluetooth, mobile phones, global positioning systems, and wireless local area networks. For mass sensor applications, the sensing technology and mechanism of BAW is similar to a quartz crystal microbalance (QCM).(1) Sauerbrey's formula describes the relationships between the mass loading and the oscillation or resonant frequency, giving a view of the sensors dependent on the gravimetric method.(2) BAW resonators comprise a piezoelectric layer interposed between two electrodes attached to a substrate.(3) Three techniques are used to fabricate an acoustic isolation zone: surface micromachining, bulk micromachining, and the use of a reflector of alternate high and low acoustic impedances. The dissipation of acoustic energy into the substrate depends on acoustic resonant isolation. A BAW resonator with a cavity-isolated structure is known as a film BAW resonator; a solidly mounted resonator (SMR) can be manufactured without micromachining.

The resonator device using surface micromachining has occupied nearly the entire BAW device market. Both processes of surface micromachining and backside etching require etching the unwanted part, which is a relatively expensive and very complex fabrication process.(4–9) Moreover, the SMR device is attracting attention because of its simple structure that includes a substrate,

*Corresponding author: e-mail: kks@stu.edu.tw
http://dx.doi.org/10.18494/SAM.2017.1522

ISSN 0914-4935

Bragg reflector, electrode, and piezoelectric layer manufactured through a process that is compatible with the IC industry.[10–12] It has the following advantages: it is manufactured through planar processes and possesses a robust structure. Therefore, an SMR was investigated in this study.

Maintaining a competitive edge through efficient product design, modeling, simulation, and other computational methods is crucial.[13] The Mason and Butterworth–Van Dyke (BVD) model equivalent circuits are used for determining the material parameters and resonance performance of a piezoelectric device.[14] By controlling each parameter, the effects of piezoelectric film thickness, material properties, or even the electrode active area on SMR performance can be investigated.

Despite the use of various piezoelectric films in transducer devices, including lead zirconate titanate, zinc oxide (ZnO), and aluminum nitride (AlN) thin films, most studies on piezoelectric thin films have focused on ZnO and AlN thin films. This study focused on AlN piezoelectric thin films because of their excellent piezoelectric properties including a high acoustic wave velocity of 10400 m/s. For the electrodes, several types of material were selected for resonant frequency tuning. In addition, the impedance influences of active area variations were simulated.

2. Modeling, Simulation, and Fabrication

2.1 Design and fabrication of the Mason model equivalent circuit for the SMR device

Figure 1 shows the structure of the SMR device, the Mason model, and the BVD model equivalent circuit of the SMR device.[15] The SMR structure comprises a piezoelectric layer interposed between two electrodes on a Bragg reflector attached to a substrate. Various physical properties of the device influence the resonant frequency performance. Therefore, different materials, material thicknesses, and resonant area sizes lead to frequency variations. Material parameters such as density, stress constant, and dielectric constant are considered in the Mason model. In this study, the SMR device was designed and simulated using the Mason model. The Bragg reflector was constructed using SiO_2 and Mo to form a high–low acoustic impedance layer. AlN and Pt/Ti were used as the piezoelectric layer and electrode, respectively. Therefore, the

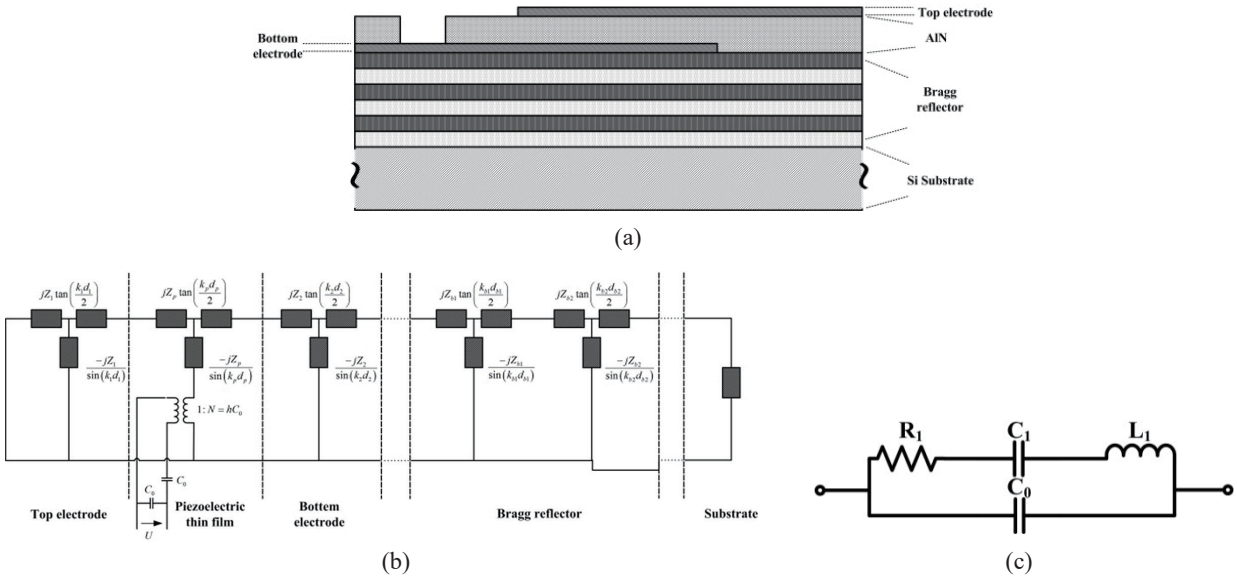

Fig. 1. (a) Schematic of an SMR, (b) Mason model, and (c) BVD model equivalent circuit of an SMR device.

structure of the Pt/Ti/AlN/Pt/Ti/Bragg reflector/Si substrate constituted an SMR device. Moreover, an SMR filter was constructed using two upward resonators. The SMR filter was simulated using the BVD model equivalent circuit through RLC, which was composed of parasitic capacitance (C_0), dynamic capacitance (C_1), dynamic inductor (L_1), and acoustic wave loss (R_1). The single-stage ladder-type SMR filter can be constructed using one parallel and two series SMR devices; moreover, the influence of various stages of the ladder-type SMR filter was investigated in this study

2.2 Fabrication of the SMR device

The low surface roughness of the Bragg reflector is a crucial factor for avoiding wave energy dissipation into the substrate. Moreover, the high c-axis orientation of a crystal is the ideal piezoelectric characteristic of an SMR device.[16] Therefore, a Bragg reflector with low surface roughness and AlN thin films with high c-axis orientation were used in our previous study.[17,18] In this study, the SiO_2 and Mo thin films were deposited on the Si substrate with the Bragg reflector through DC and RF sputtering. When the Bragg reflector was completed, the bottom electrodes were fabricated on the Bragg reflector through DC and RF sputtering combined with the mask lift-off method. The AlN piezoelectric thin films were then established on the bottom electrode through reactive RF magnetron sputtering. Finally, a G-S-G-type top electrode was constructed on the AlN piezoelectric thin films by the mask lift-off method; the SMR device was then completed.

3. Results and Discussion

3.1 Simulation and fabrication of the SMR device

In this study, the SMR device was designed and simulated using the Mason model. The Bragg reflector was constructed using SiO_2 and Mo to form a high–low acoustic impedance layer. First, AlN and Pt/Ti were used as the piezoelectric layer and electrode, respectively. Therefore, the structure of the Pt/Ti/AlN/Pt/Ti/Bragg reflector/Si substrate constituted an SMR device. For the SMR device, the thicknesses of the piezoelectric thin films and qualities of the top electrodes have been recognized as the major controlling parameters.[19–22] Therefore, the initial simulation parameters of piezoelectric thin films and top electrodes were calculated for a resonant frequency of 2503 MHz; the resonant frequency of the SMR device is shown in Fig. 2(a). The SMR device

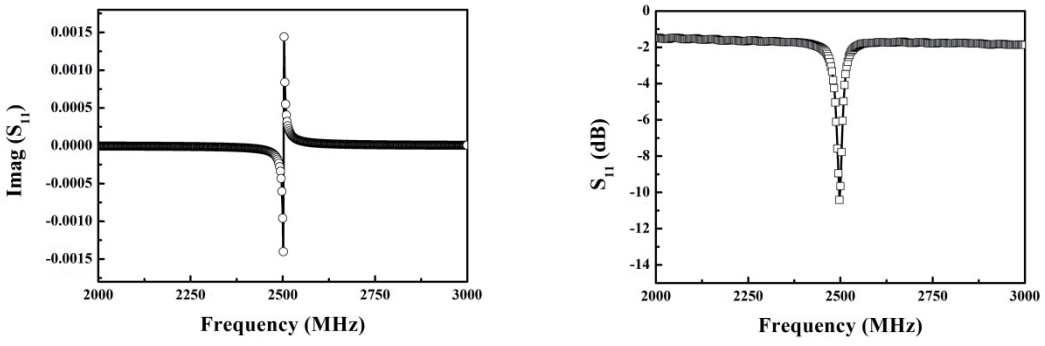

(a) (b)

Fig. 2. Resonant frequencies of (a) simulated SMR device and (b) fabricated SMR device.

was fabricated according to the simulation parameters such as the thicknesses of piezoelectric thin films and top electrodes; the resonant frequency of the SMR device can be obtained at 2497 MHz, as shown in Fig. 2(b).

3.2 Various top electrode materials and thicknesses

According to relevant literature, the mass density of a top electrode causes frequency response variation in the SMR device.[23] Therefore, various top electrode materials and different thicknesses were investigated using the Mason model. First, Pt, W, Ag, Mo, and Al were adopted as the top electrodes of the SMR device for examining the influence of resonant frequency. The simulation results for the same thickness (100 nm) of various top electrodes are shown in Fig. 3(a); the resonant frequencies of Pt, W, Ag, Mo, and Al were 2545, 2688, 2901, 2984, and 3426 MHz, respectively, and their corresponding mass densities were 21500, 19100, 10600, 10200, and 2700 kg/m^3; therefore, the larger mass density of the material reduces the resonant frequency.

Second, the top electrodes with various thicknesses were investigated to obtain the designed resonant frequency. General electrode materials such as Pt, Mo, and Al, have been widely used in semiconductor industries. Therefore, various thicknesses of Pt, Mo, and Al were used in the Mason model. Figure 3(b) shows that the increased thicknesses of the top electrodes reduce the resonant frequency because of the mass loading effect. The resonant frequency of the SMR can be designed and controlled by the selection of top electrode materials and their thicknesses. The simulation and fabrication results for various thicknesses of the Pt top electrodes are shown in Figs. 4(a) and 4(b). The increased thicknesses of the Pt thin films reduce the resonant frequency; the fabrication results conform to the simulation results.

The SMR filter comprises at least two resonators. Single-stage ladder-type SMR filters were simulated and fabricated in this study. The simulation and fabrication results in Fig. 5 show the 3 dB bandwidths of 82 and 84 MHz and insertion losses of −0.1385 and −14.67 dB, respectively. The poor outside passband of the fabricated single-stage SMR filter is prompted by the electrical loss of the bottom electrode and the electrode's interconnection. Moreover, a large deviation of the passband characteristic of the SMR filter is also clearly observed. This deviation is attributable to the poor quality of the AlN thin films.[24]

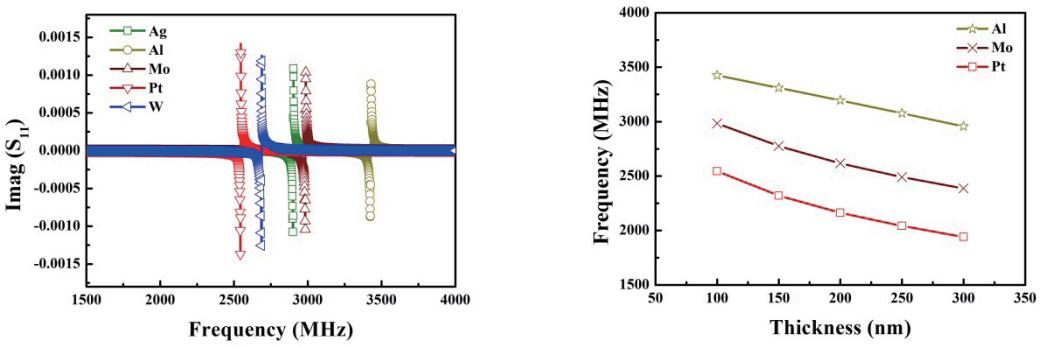

(a) (b)

Fig. 3. (Color online) (a) Frequency responses of the resonator for various types of material and (b) frequency variations for different electrode thicknesses.

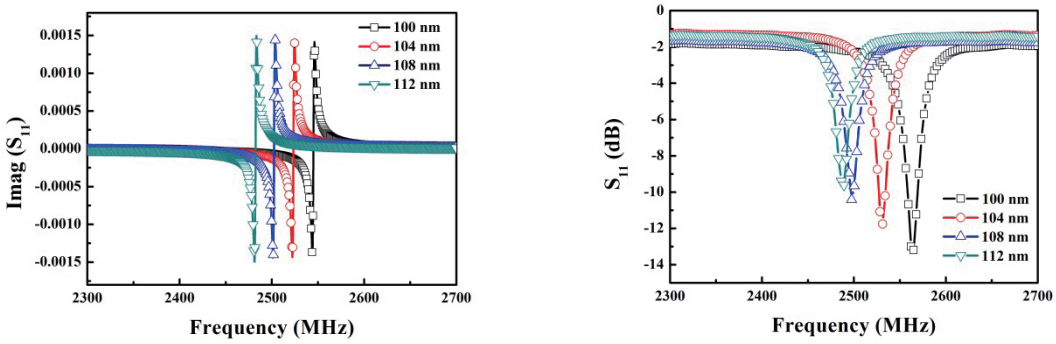

(a) (b)

Fig. 4. (Color online) Frequency responses of the resonator for various Pt electrode thicknesses: (a) simulation results and (b) fabrication results.

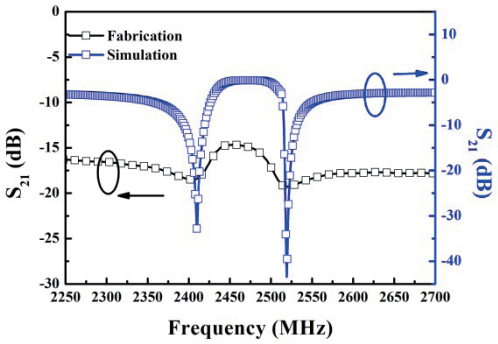

Fig. 5. (Color online) Insertion loss (S_{21}) of the single-stage ladder-type SMR filter.

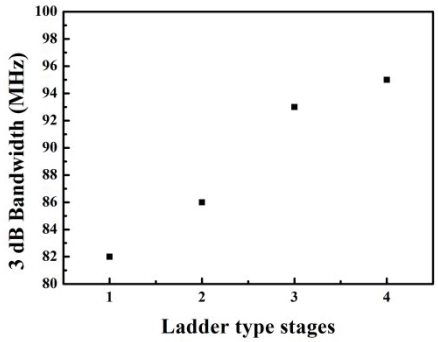

Fig. 6. 3 dB bandwidth of the ladder-type SMR filter influenced by the connection stages.

The performance of the SMR filters can be controlled through the association of resonators in series and parallel; therefore, various stages of the SMR filter were simulated. Figure 6 shows that the bandwidth increases as the number of stages increases and presents a linear trend; however, the higher number of stages increases the manufacturing cost and device area. Therefore, the manufacturing expense must be considered.

4. Conclusions

In summary, the SMR device structure comprises a piezoelectric layer interposed between two electrodes on a Bragg reflector attached to a substrate. The influence of mass loading on the resonant frequency of the simulated and fabricated SMR devices was examined. Various top electrode materials were adopted for examining the influence of resonant frequency; the result indicated that the larger mass density of the material reduces the resonant frequency. Moreover, the increased thicknesses of the top electrodes reduce the resonant frequency of the SMR because of the mass loading effect. The resonant frequency of the SMR can be designed and controlled

through the selection of top electrode materials and their thicknesses. Moreover, the results of the fabricated top electrodes with various thicknesses were compared with the simulation results. The results revealed that the increased material thickness increases the mass loading on the simulated and fabricated SMR devices, reducing the resonant frequency.

Single-stage ladder-type SMR filters comprising one parallel and two series resonators were simulated and fabricated. Within a reasonable manufacturing cost, increasing the stages of a ladder-type SMR filter produces a linear trend with respect to the bandwidth increment.

Acknowledgements

The authors gratefully acknowledge financial support from the Ministry of Science and Technology, Taiwan, R.O.C. (MOST Grant Numbers: No. MOST 103-2221-E-110-075-MY2, MOST 103-2221-E-237-006-MY2, and MOST 105-2632-E-366-001).

References

1 S. J. Martin, V. E. Granstaff, and G. C. Frye: Anal. Chem. **63** (1991) 2272.
2 G. Sauerbrey: Z. Phys. **155** (1959) 206.
3 M. Clement, J. Olivares, E. Iborra, S. González-Castilla, N. Rimmer, and A. Rastogi: Thin Solid Films **517** (2009) 4673.
4 R. C. Ruby, P. Bradley, Y. Oshmyansky, and A. Chien: IEEE Ultrasonics Symposium 2001.
5 J. D. Larson, R. C. Ruby, P. D. Bradley, J. Wen, S. L. Kok, and A. Chien: IEEE Ultrasonics Symp. (2000).
6 L. Qin, Q. Chen, H. Cheng, and Q. M. Wang: IEEE Trans. Ultrason. Ferroelectr. **57** (2010) 1840.
7 Y. C. Chen: J. Optoelectron. Adv. Mater. **12** (2010) 1993.
8 R. C. Lin, Y. C. Chen, and K. S. Kao: Appl. Phys. A **89** (2007) 475.
9 R. C. Lin, K. S. Kao, C. C. Cheng, and Y. C Chen: Thin Solid Films **516** (2008) 5262.
10 C. J. Chung, Y. C. Chen, C. C. Cheng, C. L. Wei, and K. S. Kao: IEEE Trans. Ultrason. Ferroelectr. **54** (2007) 802.
11 S. H. Lee, K. H. Yoon, and J. K. Lee: J. Appl. Phys. **92** (2002) 4062.
12 C. J. Chung, Y. C. Chen, C. C. Cheng, and K. S. Kao: IEEE Trans. Ultrason. Ferroelectr. **55** (2008) 857.
13 R. Lanz, and P. Muralt: IEEE Trans. Ultrason. Ferroelectr. **52** (2005) 938.
14 C. M. Fang, S. Y. Pao, C. Y. Lee, Y. C. Lu, P. Y. Chen, Y. C. Chin, and P. Z. Chang: J. Micro-Nanolith. MEM. **8** (2009) 021121.
15 D. Cannatà, M. Benetti, F. D. Pietrantonio, E. Verona, A. Palla-Papavlu, V. Dinca, M. Dinescu, and T. Lippert: Sens. Actuators, B **173** (2012) 32.
16 Y. C. Chen, W. C Shih, W. T. Chang, C. H. Yang, K. S. Kao, and C. C. Cheng: Nanoscale Res. Lett. **10**:69 (2015) 1.
17 W. C. Shih, Y. C. Chen, W. T. Chang, C. Y. Wen, K. S. Kao, C. C. Cheng, P. W. Ting, and J. Y. Chang: Int. Conf. Applied System Innovation (Osaka, 2015).
18 W. C. Shih, Y. C. Chen, P. W. Ting, K. S. Kao, C. C. Cheng, and W. T. Chang: Int. Electron Devices and Materials Symp. (Tainan, 2015).
19 C. L. Huang, K. W. Tay, and L. Wu: Mater. Lett. **59** (2005) 1012.
20 G. Wingqvist, J. Bjurström, L. Liljeholm, V. Yantchev, and I. Katardjiev: Sens. Actuators, B **123** (2007) 466.
21 K. W. Tay, C. L. Huang, and L. Wu: Jpn. J. Appl. Phys. **43** (2004) 1122.
22 W. Pang, H. Zhang, and E. S. Kim: IEEE Trans. Ultrason. Ferroelectr. **52** (2005) 1239.
23 R. C. Lin, Y. C. Chen, W. T. Chang, C. C. Cheng, and K. S. Kao: Sens. Actuators, A **147** (2008) 425.
24 R. Lanz and P. Muralt: IEEE Ultrasonics Symp. (2003).